Correction to Spectroscopic and Luminescence Studies on Square-Planar Platinum(II) Complexes with Anionic Tridentate 3-Bis(2-pyridineimino)isoindoline Derivatives.

ARTICLE *in* INORGANIC CHEMISTRY · MARCH 2010

Impact Factor: 4.76 · DOI: 10.1021/ic1005133 · Source: PubMed

6 AUTHORS, INCLUDING:

Hui-Min Wen

University of Texas at San Antonio

32 PUBLICATIONS **479** CITATIONS

SEE PROFILE

Zhong-Ning Chen

Chinese Academy of Sciences

179 PUBLICATIONS **3,817** CITATIONS

SEE PROFILE

2210 *Inorg. Chem.* **2010**, *49*, 2210–2221
DOI: 10.1021/ic902019s

Inorganic Chemistry
Article

Spectroscopic and Luminescence Studies on Square-Planar Platinum(II) Complexes with Anionic Tridentate 3-Bis(2-pyridylimino)isoindoline Derivatives

Hui-Min Wen,[†] Yu-Hui Wu,[†] Yang Fan,[†] Li-Yi Zhang,[†] Chang-Neng Chen,*[,†] and Zhong-Ning Chen*[,†,‡]

[†]*State Key Laboratory of Structural Chemistry, Fujian Institute of Research on the Structure of Matter and Graduate School of CAS, Chinese Academy of Sciences, Fuzhou, Fujian 350002, China, and* [‡]*State Key Laboratory of Organometallic Chemistry, Shanghai Institute of Organic Chemistry, Chinese Academy of Sciences, Shanghai 200032, China*

Received October 13, 2009

Reactions of 1,3-bis(2-pyridylimino)isoindoline (HL1), 1,3-bis(2-pyridylimino)benz(*f*)isoindoline (HL2), or 5,6-dihydro-2,3-diphenyl-5-(pyridin-2-ylimino)pyrrolo[3,4-*b*]pyrazin-7-ylidene)pyridin-2-amine (HL3) with $Pt(tht)_2Cl_2$ (tht = tetrahydrothiophene) afforded the corresponding Pt(L)Cl complexes. A series of neutral platinum(II) alkynyl complexes Pt(L)(C≡CR) were prepared by reactions of the precursors Pt(L)Cl with alkynyl ligands through CuI-catalyzed platinum acetylide σ coordination. Crystal structural determination of Pt(L3)Cl (**3**), Pt(L1)(C≡CPh) (**4**), and Pt(L1)($C{\equiv}CC_6H_4Bu^t$-4) (**6**) by X-ray crystallography revealed that the neutral platinum(Π) complexes with monoanionic tridentate L ligands display more perfect square-planar geometry than that in platinum(II) complexes with neutral tridentate 2,2′:6′,2″-terpyridyl ligands. Both the Pt(L)Cl and Pt(L)($C{\equiv}CC_6H_4R$-4) complexes exhibit low-energy absorption at 400−550 nm, arising primarily from $\pi \rightarrow \pi^*$(L) intraligand (IL) and 5d(Pt) $\rightarrow \pi^*$(L) metal-to-ligand charge-transfer (MLCT) transitions as suggested from density functional theory calculations. They display bright-orange to red room-temperature luminescence in fluid dichloromethane solutions with microsecond to submicrosecond ranges of emissive lifetimes and 0.03−3.79% quantum yields, originating mainly from ^{3}IL and ^{3}MLCT excited states. Compared with the emissive state in Pt(L)Cl complexes, substitution of the coordinated Cl with $C{\equiv}CC_6H_4R$-4 in Pt(L)($C{\equiv}CC_6H_4R$-4) complexes induces an obviously enhanced contribution from the $^3[\pi$-($C{\equiv}CC_6H_4R$-4) $\rightarrow \pi^*$(L)] ligand-to-ligand charge-transfer (LLCT) triplet state. The photophysical properties can be finely tuned by modifying both the L and alkynyl ligands. The calculated absorption and emission spectra in dichloromethane coincide well with those measured in a fluid dichloromethane solution at ambient temperature.

Introduction

Square-planar platinum(II) complexes with tridentate chelating ligands have been attracting great attention over the last few years in view of their intriguing spectroscopic and photophysical properties.[1−3] They afford extensive applications in ion sensor,[1c] luminescence signaling studies of biological interest,[4] photocatalytic hydrogen production,[5] and light-emitting materials.[6] These planar platinum(II) complexes can be aggregated along the vertical direction by intermolecular $\pi-\pi$ and Pt−Pt interactions, resulting in

*To whom correspondence should be addressed. E-mail: czn@fjirsm.ac.cn (Z.-N.C.), ccn@fjirsm.ac.cn (C.-N.C.).

(1) (a) Eryazici, I.; Moorefield, C. N.; Newkome, G. R. *Chem. Rev*. **2008**, *108*, 1834–1895. (b) Castellano, F. N.; Pomestchenko, I. E.; Shikhova, E.; Hua, F.; Muro, M. L.; Rajapakse, N. *Coord. Chem. Rev*. **2006**, *250*, 1819–1828. (c) Wong, K. M. C.; Yam, V. W. W. *Coord. Chem. Rev*. **2007**, *251*, 2477–2488. (d) Ziessel, R.; Diring, S. *Tetrahedron Lett*. **2006**, *47*, 4687–4692.

(2) (a) Yam, V. W.-W.; Tang, R. P.-L.; Wong, K. M.-C.; Cheung, K.-K. *Organometallics* **2001**, *20*, 4476–4482. (b) Zhang, H.; Zhang, B.; Li, Y.; Sun, W. *Inorg. Chem*. **2009**, *48*, 3617–3627. (c) Muro, M. L.; Castellano, F. N. *Dalton Trans*. **2007**, 4659–4665. (d) Tam, A. Y.-Y.; Lam, W. H.; Wong, K. M.-C.; Zhu, N.; Yam, V. W.-W. *Chem.—Eur. J*. **2008**, *14*, 4562–4576. (e) Wang, K.; Haga, M.-a.; Monjushiro, H.; Akiba, M.; Sasaki, Y. *Inorg. Chem*. **2000**, *39*, 4022–4028. (f) Willison, S. A.; Jude, H.; Antonelli, R. M.; Rennekamp, J. M.; Eckert, N. A.; Bauer, J. A. K.; Connick, W. B. *Inorg. Chem*. **2004**, *43*, 2548–2555.

(3) (a) Zhou, X.; Zhang, H.-X.; Pan, Q.-J.; Xia, B.-H.; Tang, A.-C. *J. Phys. Chem. A* **2005**, *109*, 8809–8818. (b) Zhou, X.; Pan, Q.-J.; Liu, T.; Li, M.-X.; Zhang, H.-X. *THEOCHEM* **2008**, *863*, 91–98. (c) Moore, J. J.; Nash, J. J.; Fanwick, P. E.; McMillin, D. R. *Inorg. Chem*. **2002**, *41*, 6387–6396. (d) Shi, L. L.; Li, T.; Zhao, S. S.; Li, H.; Su, Z. *Theor. Chem. Acc*. **2009**, *124*, 29–36.

(4) (a) Cummings, S. D. *Coord. Chem. Rev*. **2009**, *253*, 1495–1516. (b) Ma, D.-L.; Shum, T. Y.-T.; Zhang, F.; Che, C.-M.; Yang, M. *Chem. Commun*. **2005**, 4675–4677. (c) Clark, M. L.; Green, R. L.; Johnson, O. E.; Fanwick, P. E.; McMillin, D. R. *Inorg. Chem*. **2008**, *47*, 9410–9418. (d) Wu, P.; Wong, E. L. M.; Ma, D. L.; Tong, G. S. M.; Ng, K. M.; Che, C. M. *Chem.—Eur. J*. **2009**, *15*, 3652–3656.

(5) (a) Du, P.; Schneider, J.; Li, F.; Zhao, W.; Patel, U.; Castellano, F. N.; Eisenberg, R. *J. Am. Chem. Soc*. **2008**, *130*, 5056–5058. (b) Du, P.; Knowles, K.; Eisenberg, R. *J. Am. Chem. Soc*. **2008**, *130*, 12576–12577. (c) Zhang, D.; Wu, L.-Z.; Zhou, L.; Han, X.; Yang, Q.-Z.; Zhang, L.-P.; Tung, C.-H. *J. Am. Chem. Soc*. **2004**, *126*, 3440–3441. (d) Han, X.; Wu, L. Z.; Si, G.; Pan, J.; Yang, Q. Z.; Zhang, L. P.; Tung, C. H. *Chem.—Eur. J*. **2007**, *13*, 1231–1239. (e) Okazaki, R.; Masaoka, S.; Sakai, K. *Dalton Trans*. **2009**, 6127–6133.

(6) (a) Lu, W.; Mi, B. X.; Chan, M. C. W.; Hui, Z.; Che, C. M.; Zhu, N. Y.; Lee, S. T. *J. Am. Chem. Soc*. **2004**, *126*, 4958–4971. (b) Yu, C.; Chan, K. H.-Y.; Wong, K. M.-C.; Yam, V. W.-W. *Chem.—Eur. J*. **2008**, *14*, 4577–4584.

Published on Web 01/27/2010

various morphologies[7] and vapor-induced luminescence changes,[8] as well as intriguing spectroscopic and luminescence properties in both monomers and aggregates.[9] Various types of tridentate chelating ligands with N^N^N,[10] N^N^C,[4c,11] C^N^C,[12] or N^C^N[13] donors have been used to synthesize planar platinum(II) complexes.

The 3-bis(2-pyridylimino)isoindoline (BPI) derivatives have been investigated regarding their coordination chemistry to transition-metal ions,[14−17] in which they behave mostly as monoanionic N^N^N tridentate ligands. A series of platinum(II) and palladium(II) complexes with BPI ligands have been synthesized, and some of them show catalytic properties.[16,17] The X-ray crystallographic studies on palladium(II)[16,17] and platinum(II) complexes[17a] with BPI ligands show that the geometry around the platinum(II) center is closer to that of the ideal square-planar structure with better molecular rigidity than platinum(II) complexes with other tridentate N^N^N ligands.[10]

It is expected that radiationless decay can be highly constrained because of better square-planar structures in the platinum(II) complexes with 3-bis(2-pyridylimino)isoindoline derivatives, thus increasing the emissive efficiency. To our knowledge, comprehensive studies on the spectroscopic and photophysical properties concerning planar platinum(II) complexes with BPI derivatives have been unexplored. We describe herein a systematic study on the synthesis, characterization, and spectroscopic and photophysical properties of square-planar platinum(II) complexes with 3-bis(2-pyridylimino)isoindoline (HL1), 1,3-bis(2-pyridylimino)benz(*f*)isoindoline (HL2), or 5,6-dihydro-2,3-diphenyl-5-(pyridin-2-ylimino)pyrrolo[3,4-*b*]pyrazin-7-ylidene)pyridin-2-amine (HL3).

Experimental Section

General Procedures and Materials. All manipulations were performed under an argon atmosphere using standard Schlenk techniques and vacuum-line systems. Solvents were dried by standard methods and distilled prior to use except for those of spectroscopic grade for spectroscopic measurements. [(4-Methoxyphenyl)ethynyl]trimethylsilane ($Me_3SiC{\equiv}CC_6H_4OMe$-4), [(4-nitrophenyl)ethynyl]trimethylsilane ($Me_3SiC{\equiv}CC_6H_4NO_2$-4), and [[4-(trifluoromethyl)phenyl]ethynyl]trimethylsilane ($Me_3SiC{\equiv}CC_6H_4F$-4) were synthesized by Sonogashira coupling reactions.[18] 1,3-Bis(2-pyridylimino)isoindoline (HL1),[17a] 2,3-dicyanonaphthalene,[19a] 1,3-diiminobenz(*f*)isoindoline,[19b] 2,3-dicyano-5,6-diphenylpyrazine,[19c] and $Pt(tht)_2Cl_2$[20] were prepared according to literature procedures. Pt(L1)Cl (**1**) was prepared by modification of the literature method.[17a] Other chemicals were commercially available and used as received.

1,3-Bis(2-pyridylimino)benz(*f*)isoindoline (HL2). A mixture of 1,3-diiminobenz(*f*)isoindoline (500 mg, 2.56 mmol), 2-aminopyridine (506 mg, 5.38 mmol), and $CaCl_2$ (28 mg, 0.25 mmol) in 1-butanol (20 mL) was refluxed for 1 day. After cooling to room temperature, the resulting yellow precipitate was filtered off, washed with hexane, and dried in vacuo. The crude product was purified by chromatography on a silica gel column using dichloromethane/acetone (100:1) as the eluent. Yield: 60%. ESI-MS: m/z (%) 350.0 (100) $[M + 1]^+$. ^{1}H NMR ($CDCl_3$): δ 14.36 (1H, s, N−H), 8.64 (2H, d, J = 5.0 Hz, pyridine H-6), 8.63 (2H, s, naphthalene), 8.05−8.07 (2H, m, naphthalene), 7.79 (2H, t, J = 7.7 Hz, pyridine H-4), 7.61−7.64 (2H, m, naphthalene), 7.50 (2H, J = 8.0 Hz, pyridine H-3), 7.12−7.15 (2H, m, pyridine H-5).

5,6-Dihydro-2,3-diphenyl-5-(pyridin-2-ylimino)pyrrolo[3,4-*b*]-pyrazin-7-ylidene)pyridin-2-amine (HL3). This compound was synthesized by synthetic procedures similar to those of HL1.[17a] A mixture of 2,3-dicyano-5,6-diphenylpyrazine (2 g, 7.08 mol), 2-aminopyridine (1.4 g, 14.88 mol), and $CaCl_2$ (78.6 mg, 0.71 mmol) in 1-butanol (50 mL) was refluxed for 1 day. After cooling to room temperature, the resulting yellow precipitate was filtered off, washed with hexane, and dried in vacuo. The green crude product was purified by chromatography on a silica gel column using dichloromethane/methanol (200:1) as the eluent. Yield: 53%. ESI-MS: m/z (%) 454.1 (100) $[M + 1]^+$. ^{1}H NMR ($CDCl_3$): δ 14.52 (1H, s, N−H), 8.69 (2H, dd, J_1 = 4.9 Hz, J_2 = 1.3 Hz, pyridine H-6), 7.82 (2H, t, J_1 = 7.7 Hz, J_2 = 2.0 Hz, pyridine H-4), 7.69 (2H, d, J = 8.0 Hz, pyridine H-3), 7.59 (4H, dd, J_1 = 7.9 Hz, J_2 = 1.6 Hz, Ph), 7.30−7.37 (6H, m, Ph and pyridine H-5), 7.18−7.21 (2H, dd, J_1 = 7.3 Hz, J_2 = 4.9 Hz, Ph).

(7) Field, J. S.; Ledwaba, L. P.; Munro, O. Q.; McMillin, D. R. *CrystEngComm* **2008**, *10*, 740–747.
(8) (a) Wadas, T. J.; Wang, Q.-M.; Kim, Y.-j.; Flaschenreim, C.; Blanton, T. N.; Eisenberg, R. *J. Am. Chem. Soc.* **2004**, *126*, 16841–16849. (b) Du, P. W.; Schneider, J.; Brennessel, W. W.; Eisenberg, R. *Inorg. Chem.* **2008**, *47*, 69–77. (c) Grove, L. J.; Rennekamp, J. M.; Jude, H.; Connick, W. B. *J. Am. Chem. Soc.* **2004**, *126*, 1594–1595. (d) Yam, V. W.-W.; Wong, K. M.-C.; Zhu, N. Y. *J. Am. Chem. Soc.* **2002**, *124*, 6506–6507.
(9) (a) Lu, W.; Chan, M. C. W.; Zhu, N. Y.; Che, C. M.; Li, C. N.; Hui, Z. *J. Am. Chem. Soc.* **2004**, *126*, 7639–7651. (b) Chan, K. H.-Y.; Lam, J. W.-Y.; Wong, K. M.-C.; Tang, B.-Z.; Yam, V. W.-W. *Chem.—Eur. J.* **2009**, *15*, 2328–2334.
(10) (a) Tong, W.-L.; Chan, M. C. W.; Zhu, N.; Leung, S.-K. *Dalton Trans.* **2009**, 4741–4746. (b) Jarosz, P.; Lotito, K.; Schneider, J.; Kumaresan, D.; Schmehl, R.; Eisenberg, R. *Inorg. Chem.* **2009**, *48*, 2420–2428. (c) Rachford, A. A.; Goeb, S.; Ziessel, R.; Castellano, F. N. *Inorg. Chem.* **2008**, *47*, 4348–4355. (d) Shikhova, E.; Danilov, E. O.; Kinayyigit, S.; Pomestchenko, I. E.; Tregubov, A. D.; Camerel, F.; Retailleau, P.; Ziessel, R.; Castellano, F. N. *Inorg. Chem.* **2007**, *46*, 3038–3048. (e) Field, J. S.; Haines, R. J.; Ledwaba, L. P.; McGuire, R.; Munro, O. Q.; Low, M. R.; McMillin, D. R. *Dalton Trans.* **2007**, 192–199.
(11) (a) Lai, S.-W.; Lam, H.-W.; Lu, W.; Cheung, K.-K.; Che, C.-M. *Organometallics* **2002**, *21*, 226–234. (b) Clark, M. L.; Diring, S.; Retailleau, P.; McMillin, D. R.; Ziessel, R. *Chem.—Eur. J.* **2008**, *24*, 7168–7179. (c) Lai, S.-W.; Chan, M. C.-W.; Cheung, T.-C.; Peng, S.-M.; Che, C.-M. *Inorg. Chem.* **1999**, *38*, 4046–4055.
(12) (a) Yam, V. W.-W.; Tang, R. P.-L.; Wong, K. M.-C.; Lu, X.-X.; Cheung, K.-K.; Zhu, N. *Chem.—Eur. J.* **2008**, *14*, 4066–4076. (b) Berenguer, J. R.; Lalinde, E.; Torroba, J. *Inorg. Chem.* **2007**, *46*, 9919–9930. (c) Camerel, F.; Ziessel, R.; Donnio, B.; Bourgogne, C.; Guillon, D.; Schmutz, M.; Iacovita, C.; Bucher, J. P. *Angew. Chem., Int. Ed.* **2007**, *46*, 2659–2662.
(13) (a) Williams, J. A. G. *Chem. Soc. Rev.* **2009**, *38*, 1783–1801. (b) Develay, S.; Williams, J. A. G. *Dalton Trans.* **2008**, 4562–4564. (c) Lu, W.; Law, Y.-C.; Han, J.; Chui, S. S.-Y.; Ma, D.-L.; Zhu, N.-Y.; Che, C.-M. *Chem. Asian J.* **2008**, *3*, 59–69.
(14) Dietrich, B. L.; Egbert, J.; Morris, A. M.; Wicholas, M.; Anderson, O. P.; Miller, S. M. *Inorg. Chem.* **2005**, *44*, 6476–6481.
(15) (a) Anderson, O. P.; la Cour, A.; Dodd, A.; Garrett, A. D.; Wicholas, M. *Inorg. Chem.* **2003**, *42*, 122–127. (b) Wicholas, M.; Garrett, A. D.; Gleaves, M.; Morris, A. M.; Rehm, M.; Anderson, O. P.; la Cour, A. *Inorg. Chem.* **2006**, *45*, 5804–5811.
(16) (a) Bröring, M.; Kleeberg, C. *Dalton Trans.* **2007**, 1101–1103. (b) Bröring, M.; Kleeberg, C.; Tejero, E. C. *Eur. J. Inorg. Chem.* **2007**, 3208–3216. (c) Broring, M.; Kleeberg, C.; Kohler, S. *Inorg. Chem.* **2008**, *47*, 6404–6412. (d) Bröring, M.; Kleeberg, C. *Z. Anorg. Allg. Chem.* **2007**, *633*, 2210–2216.
(17) (a) Meder, M.; Galka, C. H.; Gade, L. H. *Monatsh. Chem.* **2005**, *136*, 1693–1706. (b) Siggelkow, B.; Meder, M. B.; Galka, C. H.; Gade, L. H. *Eur. J. Inorg. Chem.* **2004**, 3424–3435. (c) Meder, M. B.; Gade, L. H. *Eur. J. Inorg. Chem.* **2004**, 2716–2722. (d) Langlotz, B. K.; Wadepohl, H.; Gade, L. H. *Angew. Chem., Int. Ed.* **2008**, *47*, 4670–4674. (e) Schilf, W. *J. Mol. Struct.* **2004**, *691*, 141–148.
(18) Takahashi, S. K. Y.; Sonogashira, K.; Hagihara, N. *Synthesis* **1980**, 627–630.
(19) (a) Baird, D. M.; Maehlmann, W. P.; Bereman, R. D.; Singh, P. *J. Coord. Chem.* **1997**, *42*, 107–126. (b) Wheeler, B. L.; Nagasubramanian, G.; Bard, A. J.; Schechtman, L. A.; Kenney, M. E. *J. Am. Chem. Soc.* **1984**, *106*, 7404–7410. (c) Cristiano, R.; Westphal, E.; Bechtold, I. H.; Bortoluzzi, A. J.; Gallardo, H. *Tetrahedron* **2007**, *63*, 2851–2858.
(20) Usón, R.; Forniés, J.; Martínez, F.; Tomás, M. *J. Chem. Soc., Dalton Trans.* **1980**, 888–894.

Pt(L2)Cl (2). A mixture of $Pt(tht)_2Cl_2$ (200 mg, 0.45 mmol), HL2 (158 mg, 0.45 mmol), and triethylamine (0.13 mL, 0.9 mmol) in 20 mL of methanol was refluxed for 12 h. After cooling to room temperature, the resulting red precipitate was filtered off, washed with water, a small amount of ethanol, and Et_2O, and dried in vacuo. The product was purified by recrystallization from dichloromethane/*n*-hexane. Yield: 80%. Anal. Calcd for $C_{22}H_{14}N_5ClPt \cdot {}^1/_4C_6H_{14}$: C, 47.01; H, 2.94; N, 11.66. Found: C, 46.61; H, 2.83; N, 11.74. ESI-MS: *m*/*z* (%) 579.3 (100) $[M + 1]^+$. ^1H NMR (DMSO): δ 10.27 (2H, d, J = 6.4 Hz, pyridine H-6), 8.54 (2H, s, naphthalene), 8.04−8.06 (2H, m, naphthalene), 7.91 (2H, t, J = 7.5 Hz, pyridine H-4), 7.58−7.61 (2H, m, naphthalene), 7.61 (2H, d, J = 7.5 Hz, pyridine H-3), 7.02 (2H, t, J = 6.9 Hz, pyridine H-5).

Pt(L3)Cl (3). This compound was prepared by the same synthetic procedure as that of **2** except that HL3 was used in place of HL2. Yield: 65%. Anal. Calcd for $C_{28}H_{18}N_7ClPt$: C, 49.24; H, 2.66; N, 14.35. Found: C, 49.18; H, 2.67; N, 14.28. ESI-MS: *m*/*z* (%) 683.2 (100) $[M + 1]^+$. ^1H NMR ($CDCl_3$): δ 10.39 (2H, dd, J_1 = 6.5 Hz, J_2 = 1.5 Hz, pyridine H-6), 8.01 (2H, td, J_1 = 7.6 Hz, J_2 = 1.6 Hz, pyridine H-4), 7.88 (2H, dd, J_1 = 8.1 Hz, J_2 = 1.5 Hz, pyridine H-3), 7.59−7.62 (4H, m, Ph−L3), 7.32−7.39 (6H, m, Ph, pyridine H-5), 7.15 (2H, td, J_1 = 5.8 Hz, J_2 = 1.8 Hz, Ph).

Pt(L1)(C≡CC$_6$H$_5$) (4). A mixture of **1** (100 mg, 0.19 mmol), phenylacetylene (0.086 mL, 0.80 mmol), CuI (10 mg, 0.05 mmol), and NEt_3 (5 mL) in dichloromethane (30 mL) was refluxed for 12 h. After cooling to room temperature, the reaction mixture was filtered and the filtrate was evaporated to dryness under reduced pressure to give a solid residue. The crude product was purified by chromatography on a silica gel column using dichloromethane as the eluent. Yield: 68%. Anal. Calcd for $C_{26}H_{17}N_5Pt$: C, 52.53; H, 2.88; N, 11.78. Found: C, 52.32; H, 2.63; N, 11.62. ESI-MS: *m*/*z* (%) 595.4 (100) $[M + 1]^+$. ^1H NMR ($CDCl_3$): δ 10.78 (2H, d, J = 5.4 Hz, pyridine H-6), 8.09−8.11 (2H, m, Ph−L1), 7.93 (2H, t, J = 6.9 Hz, pyridine H-4), 7.69 (2H, d, J = 8.0 Hz, pyridine H-3), 7.64−7.66 (2H, m, Ph−L1), 7.54 (2H, d, J = 7.2 Hz, pyridine H-5), 7.33 (2H, t, J = 7.5 Hz, C_6H_5), 7.23−7.26 (1H, m, C_6H_5), 6.96 (2H, t, J = 6.7 Hz, C_6H_5). IR (KBr disk, ν/cm^{-1}): 2113s (C≡C).

Pt(L1)(C≡CC$_6$H$_4$F-4) (5). This compound was prepared by the same synthetic procedure as that of **4**, except that (4-fluorophenyl)acetylene was used in place of phenylacetylene. Yield: 70%. Anal. Calcd for $C_{26}H_{16}FN_5Pt$: C, 50.98; H, 2.63; N, 11.43. Found: C, 50.87; H, 2.57; N, 11.52. ESI-MS: *m*/*z* (%) 613.3 (100) $[M + 1]^+$. ^1H NMR ($CDCl_3$): δ 10.72 (2H, d, J = 6.4 Hz, pyridine H-6), 8.07−8.09 (2H, m, Ph−L1), 7.92 (2H, t, J = 7.5 Hz, pyridine H-4), 7.67 (2H, d, J = 8.0 Hz, pyridine H-3), 7.63−7.68 (2H, m, Ph−L1), 7.47 (2H, t, J = 5.9 Hz, pyridine H-5), 7.01 (2H, t, J = 8.6 Hz, C_6H_4F-4), 6.95 (2H, t, J = 6.7 Hz, C_6H_4F-4). IR (KBr disk, ν/cm^{-1}): 2113s (C≡C).

Pt(L1)(C≡CC$_6$H$_4$Bu^t-4) (6). This compound was prepared by the same synthetic procedure as that of **4** except that (4-*tert*-butylphenyl)acetylene was used in place of phenylacetylene. Yield: 80%. Anal. Calcd for $C_{30}H_{25}N_5Pt \cdot {}^1/_2C_6H_{14}$: C, 57.14; H, 4.65; N, 10.10. Found: C, 57.20; H, 4.48, N, 9.77. ESI-MS: *m*/*z* (%) 651.0 (100) $[M + 1]^+$. ^1H NMR ($CDCl_3$): δ 10.80 (2H, J = 6.4 Hz, pyridine H-6), 8.09−8.11 (2H, m, Ph−L1), 7.93 (2H, t, J = 8.4 Hz, pyridine H-4), 7.69 (2H, d, J = 8.1 Hz, pyridine H-3), 7.63−7.65 (2H, m, Ph−L1), 7.49 (2H, d, J = 8.4 Hz, pyridine H-5), 7.36 (2H, d, J = 8.4 Hz, $C_6H_4Bu^t$-4), 6.95 (2H, t, J = 6.7 Hz, $C_6H_4Bu^t$-4), 1.35 (9H, s, Bu^t). IR (KBr disk, ν/cm^{-1}): 2118s (C≡C).

Pt(L1)(C≡CC$_6$H$_4$NO$_2$-4) (7). A mixture of **1** (200 mg, 0.38 mmol), [(4-nitrophenyl)ethynyl]trimethylsilane (387 mg, 1.90 mmol), CuI (4 mg, 0.02 mmol), and KF (330 mg, 5.7 mmol) in dichloromethane/methanol (2:1, v/v; 30 mL) was refluxed for 1 day. After cooling to room temperature, the reaction mixture was filtered and the filtrate was evaporated to dryness under reduced pressure to give a solid residue. The crude product was purified by chromatography on a silica gel column using dichloromethane as the eluent. Yield: 70%. Anal. Calcd for $C_{26}H_{16}N_6O_2Pt \cdot 3CH_2Cl_2$: C, 38.95; H, 2.48; N, 9.40. Found: C, 39.18; H, 2.50; N, 9.81. ESI-MS: *m*/*z* (%): 640.0 (100) $[M + 1]^+$. ^1H NMR ($CDCl_3$): δ 10.58 (2H, d, J = 6.5 Hz, pyridine H-6), 8.22 (2H, d, J = 8.8 Hz, $C_6H_4NO_2$-4), 8.12−8.14 (2H, m, Ph−L1), 7.98 (2H, t, J = 8.4 Hz, pyridine H-4), 7.75 (2H, d, J = 8.2 Hz, pyridine H-3), 7.67−7.71 (2H, m, Ph−L1), 7.59 (2H, d, J = 8.8 Hz, pyridine H-5), 7.00 (2H, t, J = 6.7 Hz, C_6H_4NO2-4). IR (KBr disk, ν/cm^{-1}): 2111s (C≡C).

Pt(L1)(C≡CC$_6$H$_4$OCH$_3$-4) (8). This compound was prepared by the same synthetic procedure as that of **7** except that [(4-methoxyphenyl)ethynyl]trimethylsilane was used in place of [(4-nitrophenyl)ethynyl]trimethylsilane. Yield: 80%. Anal. Calcd for $C_{27}H_{19}N_5OPt$: C, 51.92; H, 3.07; N, 11.21. Found: C, 52.35; H, 3.16; N, 10.89. ESI-MS: *m*/*z* (%) 625.0 (100) $[M + 1]^+$. ^1H NMR ($CDCl_3$): δ 10.81 (2H, d, J = 6.4 Hz, pyridine H-6), 8.08−8.09 (2H, m, Ph−L1), 7.93 (2H, t, J = 7.8 Hz, pyridine H-4), 7.68 (2H, d, J = 8.2 Hz, pyridine H-3), 7.63−7.65 (2H, m, Ph−L1), 7.46 (2H, d, J = 8.8 Hz, pyridine H-5), 6.96 (2H, t, J = 6.4 Hz, $C_6H_4OCH_3$-4), 6.88 (2H, d, J = 8.6 Hz, $C_6H_4OCH_3$-4), 3.83 (s, 3H, OCH_3). IR (KBr disk, ν/cm^{-1}): 2115s (C≡C).

Pt(L1)(C≡CC$_6$H$_4$CF$_3$-4) (9). This compound was prepared by the same synthetic procedure as that of **7** except that [[4-(trifluoromethyl)phenyl]ethynyl]trimethylsilane was used in place of [(4-nitrophenyl)ethynyl]trimethylsilane. Yield: 80%. Anal. Calcd for $C_{27}H_{16}F_3N_5Pt$: C, 48.95; H, 2.43; N, 10.57. Found: C, 48.90; H, 2.45; N, 10.68. ESI-MS: *m*/*z* (%) 664.0 (100) $[M + 1]^+$. ^1H NMR ($CDCl_3$): δ 10.63 (2H, d, J = 5.8 Hz, pyridine H-6), 8.07−8.09 (2H, m, Ph−L1), 7.93 (2H, t, J = 7.0 Hz, pyridine H-4), 7.68 (2H, d, J = 8.4 Hz, pyridine H-3), 7.64−7.69 (2H, m, Ph−L1), 7.57 (4H, m, pyridine H-5, C_6H_4-OCF_3-4), 6.94 (2H, t, J = 5.1 Hz, $C_6H_4OCF_3$-4). IR (KBr disk, ν/cm^{-1}): 2111s (C≡C).

Pt(L2)(C≡CC$_6$H$_4$Bu^t-4) (10). This compound was prepared by the same synthetic procedure as that of **4** except that **2** and (4-*tert*-butylphenyl)acetylene were used in place of **1** and phenylacetylene, respectively. Anal. Calcd for $C_{34}H_{27}N_5Pt \cdot {}^1/_2CH_2Cl_2$: C, 55.76; H, 3.80; N, 9.42. Found: C, 55.36; H, 3.75; N, 9.53. ESI-MS: *m*/*z* (%) 701.6 (100) $[M + 1]^+$. ^1H NMR ($CDCl_3$): δ 10.65 (2H, d, J = 5.7 Hz, pyridine H-6), 8.66 (2H, s, naphthalene), 8.26−8.29 (2H, m, naphthalene), 8.19 (2H, t, J = 7.3 Hz, pyridine H-4), 7.69−7.74 (4H, m, naphthalene, pyridine H-3), 7.34−7.39 (4H, m, pyridine H-5, $C_6H_4Bu^t$-4), 7.23 (2H, t, J = 6.2 Hz, $C_6H_4Bu^t$-4), 1.30 (9H, s, Bu^t). IR (KBr disk, ν/cm^{-1}): 2115s (C≡C).

Pt(L3)(C≡CC$_6$H$_4$Bu^t-4) (11). This compound was prepared by the same synthetic procedure as that of **4** except that **3** and (4-*tert*-butylphenyl)acetylene were used in place of **1** and phenylacetylene, respectively. Yield: 68%. Anal. Calcd for $C_{40}H_{31}N_7Pt$: C, 59.70; H, 3.88; N, 12.18. Found: C, 59.88; H, 3.79; N, 11.95. ESI-MS: *m*/*z* (%) 805.2 (100) $[M + 1]^+$. ^1H NMR (DMSO): δ 10.68 (2H, s, pyridine H-6), 8.22 (2H, t, J = 7.6 Hz, pyridine H-4), 8.02 (2H, d, J = 7.6 Hz, pyridine H-3), 7.50−7.52 (4H, m, Ph, $C_6H_4Bu^t$-4), 7.36−7.45 (10H, m, Ph, pyridine H-5), 7.28 (2H, t, J = 6.3 Hz, $C_6H_4Bu^t$-4), 1.30 (9H, s, Bu^t). IR (KBr disk, ν/cm^{-1}): 2118s (C≡C).

Physical Measurements. UV−vis absorption spectra were measured on a Perkin-Elmer Lambda 25 UV−vis spectrophotometer. IR spectra were recorded on a Magna 750 FT-IR spectrophotometer with KBr pellets. Elemental analyses (C, H, and N) were carried out on a Perkin-Elmer model 240 C elemental analyzer. Electrospray ionization mass spectrometry (ESI-MS) was performed on a Finnigan LCQ mass spectrometer using dichloromethane/methanol mixtures as mobile phases. The cyclic voltammograms (CVs) were made with a potentiostat/galvanostat model 263A in dichloromethane solutions containing 0.1 M Bu_4NPF_6 as the supporting electrolyte.

The CV was made at a scan rate of 100 mV s^{-1}. Platinum and glassy graphite were used as the counter and working electrodes, respectively, and the potential was measured against a Ag/AgCl reference electrode. The potential measured was always referenced to the half-wave potentials of the ferrocenium/ferrocene couple ($E_{1/2}$ = 0). Emission and excitation spectra were recorded on a Perkin-Elmer LS55 luminescence spectrometer with a red-sensitive photomultiplier type R928. Emission lifetimes in solid states and degassed solutions were determined on an Edinburgh analytical instrument (F900 fluorescence spectrometer) using an LED laser at 440 nm excitation. The emission quantum yield (Φ_{em}) in a degassed dichloromethane solution at room temperature was calculated by $\Phi_s = \Phi_r(B_r/B_s)(n_s/n_r)^2(D_s/D_r)$ using $[Ru(bpy)_3](PF_6)_2$ in acetonitrile as the standard (Φ_{em} = 0.062), where the subscripts r and s denote the reference standard and sample solution, respectively, and n, D, and Φ are the refractive index of the solvents, the integrated intensity, and the luminescence quantum yield, respectively. The quantity B is calculated by $B = 1 - 10^{-AL}$, where A is the absorbance at the excitation wavelength and L is the optical path length.

Crystal Structural Determination. Crystals of **3**, **4**, and **6** suitable for X-ray diffraction studies were obtained by layering *n*-hexane onto the dichloromethane solution. Data collection was performed on a Mercury CCD diffractometer by the ω-scan technique at room temperature using graphite-monochromated Mo Kα (λ = 0.710 73 Å) radiation. The *CrystalClear* software package was used for data reduction and empirical absorption correction. The structures were solved by direct methods. The heavy atoms were located from an *E*-map, and the rest of the non-hydrogen atoms were found in subsequent Fourier maps. All non-hydrogen atoms were refined anisotropically, while the hydrogen atoms were generated geometrically and refined with isotropic thermal parameters. The structures were refined on F^2 by full-matrix least-squares methods using the *SHELXTL-97* program package.[21] The crystallographic data are summarized in Table 1.

Theoretical Methodology. All of the calculations were carried out by using the *Gaussian 03* program package.[22] The density functional theory (DFT)[23] at the gradient-corrected correlation functional level PBE1PBE[24] was used to optimize the ground-state geometries of the 3-bis(2-pyridylimino)isoindoline-platinum(II) complexes **1**−**4** and **6**, giving the best results in terms of the structural parameters and simulations of the UV−vis properties by comparison of different functionals (Table S1, Supporting Information). On the basis of the ground-state optimized geometries, 80 singlet and 6 triplet excited states were obtained to determine the vertical excitation energies for all of the molecules in the dichloromethane media using the time-dependent DFT (TD-DFT) method at the same level as that mentioned previously.[25,26] The conductor-like polarizable continuum model (CPCM)[27] with dichloromethane as the solvent was used for calculations in solution. In these calculations, the Hay−Wadt double-ξ method with a Los Alamos relativistic effect basis set (LANL2DZ)[28] consisting of effective core potentials was employed for the platinum(II) atom and the 6-31G(p,d) basis set was used for the remaining atoms. To precisely describe the molecular properties, one additional f-type polarization function was implemented for the platinum(II) atom (α = 0.18)[29] and chloride atom (α = 0.514).[30]

Table 1. Crystallographic Data for **3**, **4**, and **6**

	3	**4**	**6**
empirical formula	$C_{28}H_{18}C_6N_7Pt$	$C_{26}H_{17}N_5Pt$	$C_{30}H_{25}N_5Pt$
fw	683.04	594.54	650.64
space group	$P\bar{1}$	$P\bar{1}$	$P2_1/c$
a, Å	8.591(4)	7.266(3)	10.854(5)
b, Å	9.782(4)	11.643(6)	11.573(5)
c, Å	15.367(6)	12.473(6)	20.151(10)
α, deg	74.412(16)	89.266(13)	
β, deg	74.060(16)	82.760(13)	101.016(8)
γ, deg	79.089(15)	78.324(14)	
V, Å^3	1186.7(9)	1025.0(9)	2485(2)
Z	2	2	4
ρ_{calcd}, g cm^{-3}	1.911	1.926	1.739
μ, mm^{-1}	6.058	6.870	5.676
radiation (λ, Å)	0.710 73	0.710 73	0.710 73
temp, K	293(2)	293(2)	293(2)
R1(F_o)[a]	0.0537	0.0435	0.0390
wR2(F_o^2)[b]	0.1424	0.1131	0.0834
GOF	1.075	1.002	0.999

[a] $R1 = \sum|F_o - F_c|/\sum F_o$. [b] $wR2 = \sum[w(F_o^2 - F_c^2)^2]/\sum[w(F_o^2)]^{1/2}$.

Results and Discussion

Preparation and Characterization. The BPI derivatives HL1−HL3 (Scheme 1) were synthesized by the reaction of *o*-dicarbonitrile or 1,3-diiminobenz(*f*)isoindoline (for HL2) with 2-aminopyridine in refluxing 1-butanol, using $CaCl_2$ as the catalyst.[16,17] The Pt(BPI)Cl complexes **1**−**3** (Scheme 1) were prepared by the reactions of HL1−HL3 with $Pt(tht)_2Cl_2$ in refluxing methanol using triethylamine (NEt_3) as the base. **1**−**3** were purified by recrystallization from dichloromethane/*n*-hexane. Alkynylplatinum(II) complexes **4**−**11** (Scheme 1) were obtained from the reactions of Pt(BPI)Cl complexes with the corresponding alkynes in the presence of KF or NEt_3 and a catalytic amount of CuI. They were purified by chromatography on silica gel columns. Substitution of chloride in **1**−**3** with a σ-bonded acetylide ligand increases significantly the solubility of **4**−**11** in halohydrocarbon solvents. The deprotonated BPI derivatives L1−L3 act as anionic N^N^N tridentate ligands to afford neutral platinum(II) complexes **1**−**3** with coordinated Cl or **4**−**11** containing σ-bonded acetylides.

(21) Sheldrick, G. M. *SHELXL-97, Program for the Refinement of Crystal Structures*; University of Göttingen: Göttingen, Germany, 1997.
(22) Frisch, M. J.; Trucks, G. W.; Schlegel, H. B.; Scuseria, G. E.; Robb, M. A.; Cheeseman, J. R.; Montgomery, J. A., Jr.; Vreven, T.; Kudin, K. N.; Burant, J. C.; Millam, J. M.; Iyengar, S. S.; Tomasi, J.; Barone, V.; Mennucci, B.; Cossi, M.; Scalmani, G.; Rega, N.; Petersson, G. A.; Nakatsuji, H.; Hada, M.; Ehara, M.; Toyota, K.; Fukuda, R.; Hasegawa, J.; Ishida, M.; Nakajima, T.; Honda, Y.; Kitao, O.; Nakai, H.; Klene, M.; Li, X.; Knox, J. E.; Hratchian, H. P.; Cross, J. B.; Bakken, V.; Adamo, C.; Jaramillo, J.; Gomperts, R.; Stratmann, R. E.; Yazyev, O.; Austin, A. J.; Cammi, R.; Pomelli, C.; Ochterski, J. W.; Ayala, P. Y.; Morokuma, K.; Voth, G. A.; Salvador, P.; Dannenberg, J. J.; Zakrzewski, V. G.; Dapprich, S.; Daniels, A. D.; Strain, M. C.; Farkas, O.; Malick, D. K.; Rabuck, A. D.; Raghavachari, K.; Foresman, J. B.; Ortiz, J. V.; Cui, Q.; Baboul, A. G.; Clifford, S.; Cioslowski, J.; Stefanov, B. B.; Liu, G.; Liashenko, A.; Piskorz, P.; Komaromi, I.; Martin, R. L.; Fox, D. J.; Keith, T.; Al-Laham, M. A.; Peng, C. Y.; Nanayakkara, A.; Challacombe, M.; Gill, P. M. W.; Johnson, B.; Chen, W.; Wong, M. W.; Gonzalez, C.; Pople, J. A. *Gaussian 03*, revision C.02; Gaussian, Inc.: Wallingford, CT, **2004**.
(23) Becke, A. D. *J. Chem. Phys.* **1993**, *98*, 5648–5652.
(24) Perdew, J. P.; Burke, K.; Ernzerhof, M. *Phys. Rev. Lett.* **1997**, *77*, 3865–3868.
(25) Casida, M. E.; Jamorski, C.; Casida, K. C.; Salahub, D. R. *J. Chem. Phys.* **1998**, *108*, 4439–4449.
(26) Stratmann, R. E.; Scuseria, G. E.; Frisch, M. J. *J. Chem. Phys.* **1998**, *109*, 8218–8224.
(27) (a) Barone, V.; Cossi, M. *J. Phys. Chem. A* **1998**, *102*, 1995–2001. (b) Cossi, M.; Regar, N.; Scalmani, G.; Barone, V. *J. Comput. Chem.* **2003**, *24*, 669–681.
(28) (a) Wadt, W. R.; Hay, P. J. *J. Chem. Phys.* **1985**, *82*, 284–298. (b) Hay, P. J.; Wadt, W. R. *J. Chem. Phys.* **1985**, *82*, 299–310.
(29) (a) Pyykkö, P.; Runeberg, N.; Mendizabal, F. *Chem.—Eur. J.* **1997**, *3*, 1451–1457. (b) Pyykkö, P.; Mendizabal, F. *Chem.—Eur. J.* **1997**, *3*, 1458–1465.
(30) Pyykkö, P.; Mendizabal, F. *Inorg. Chem.* **1998**, *37*, 3018–3025.

Scheme 1. Synthetic Routes to Complexes **1**−**11**

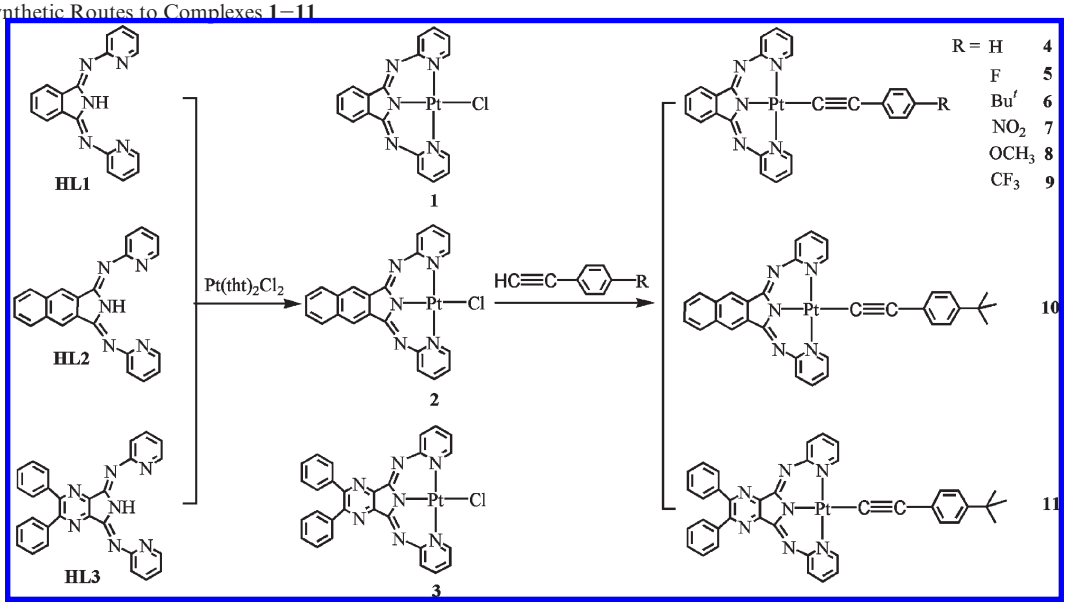

Two different morphologies were obtained in solid states with black and red forms for **4** and **5**, respectively. Complex **4** was mainly crystallized as the black form, whereas the red form was isolated as a minor product (>2%) so that the amount is insufficient for spectroscopic characterization, but the structure of the red form was determined by X-ray crystallography. The black crystals of **4** are too fragile to be characterized by X-ray crystallography. For **5**, the black form was isolated by evaporating a dichloromethane solution to dryness under reduced pressure or layering *n*-hexane onto the dichloromethane solution, while the red powder was obtained by the slow evaporation of tetrahydrofuran (THF) or a dichloromethane solution of **5**.

Complexes **1**−**11** were characterized by elemental analysis, ESI-MS spectrometry, and ^{1}H NMR and IR spectroscopies and **3**, **4**, and **6** by X-ray crystallography. Elemental analysis of C, H, and N coincided well with the calculated values for all of the compounds. Positive-ion ESI-MS of the neutral complexes showed the corresponding molecular ion peak $[M + 1]^+$ as the principal peaks. Strong ν(C≡C) frequencies were detected at 2110−2120 cm^{-1} in the IR spectra of alkynylplatinum(II) complexes **4**−**11**.

Slow diffusion of *n*-hexane into dichloromethane solutions of **3**, **4**, and **6** afforded red crystals suitable for X-ray diffraction measurements. Selected bond distances and angles are summarized in Table 2. ORTEP drawings of **3**, **4**, and **6** are depicted in Figures 1−3, respectively. A packing diagram of **3** showing an antiparallel stacking of planar platinum(II) moieties is given in Figure 1 (bottom).

Platinum(II) complexes **3**, **4**, and **6** exhibit approximately square-planar geometry composed of ClN_3 donors for **3** or CN_3 chromophores for **4** and **6**. As indicated by the adjacent and opposite angles (Table 2) around the platinum(II) atoms, the square-planar structures of **3**, **4**, and **6** are more perfect than those of related platinum(II) complexes with neutral tridentate N^N^N ligands including 2,2′:6′,2″-terpyridine (tpy),[2a,b] 2,6-bis(*N*-pyrazolyl)-pyridine (bpp),[2f] and bis(*N*-alkylbenzimidazol-2-yl)pyridines

Table 2. Selected Bond Distances [Å] and Angles [deg] for **3**, **4**, and **6**

	3	4	6
Pt−Cl/C19	2.335(2)	1.965(8)	1.978(5)
Pt−N1	2.030(6)	2.048(7)	2.051(4)
Pt−N3	1.977(6)	1.985(6)	1.995(4)
Pt−N5	2.047(6)	2.044(6)	2.049(4)
C19−C20		1.224(12)	1.195(7)
N1−Pt−Cl/C19	88.59(18)	90.8(3)	90.25(19)
N1−Pt−N3	89.9(2)	89.0(3)	89.33(17)
N1−Pt−N5	174.3(2)	175.5(2)	172.35(14)
N3−Pt−Cl/C19	172.28(17)	172.0(3)	89.33(17)
N3−Pt−N5	89.2(2)	89.8(3)	89.42(16)
N5−Pt−Cl/C19	93.01(18)	91.0(3)	92.19(19)
Pt−C19−C20		173.6(8)	174.8(5)

(bzimpy).[2d] This is readily understandable because the square-planar geometry with two six-membered chelating rings in **3**, **4**, or **6** induces significantly less constraint than that with two five-membered chelating rings in platinum(II) complexes with tridentate tpy, bpp, or bzimpy.[2−10] The Pt−C≡C angle is 173.6° for **4** and 174.8° for **5**, indicating a quasi-linear connection through σ-acetylide coordination. Of the three Pt−N bonds for the deprotonated tridentate L ligand, the central Pt−N3 [1.977(6)−1.995(4) Å] distance is obviously shorter than those of the two outer Pt−N1 [2.030(6)−2.051(4) Å] and Pt−N5 [2.044(6)−2.049(4) Å] bonds. Noticeably, the distance difference between the central and outer Pt−N bonds is more pronounced than that in platinum(II) complexes with neutral tridentate N^N^N ligands.[2−10] In striking contrast with the coplanarity between phenylacetylide and the CN_3 donor atoms in platinum(II) terpyridyl alkynyl complexes,[2a,d,f] phenylacetylide forms dihedral angles of 89.9 and 72.0° with the platinum(II) coordination plane for **4** and **6**, respectively. The Pt−C and C≡C bond distances are in the normal ranges for platinum(II) alkynyl complexes.[2a,d,f] The adjacent planar platinum(II) moieties exhibit an antiparallel packing so as to induce a severe slide from one another, as shown in Figure 1 (bottom). The shortest intermolecular Pt···Pt separations are 4.73 Å for **3**, 6.33 Å for **4**, and 4.73 Å for **6**, precluding the possibility of metallophilic Pt−Pt interactions.

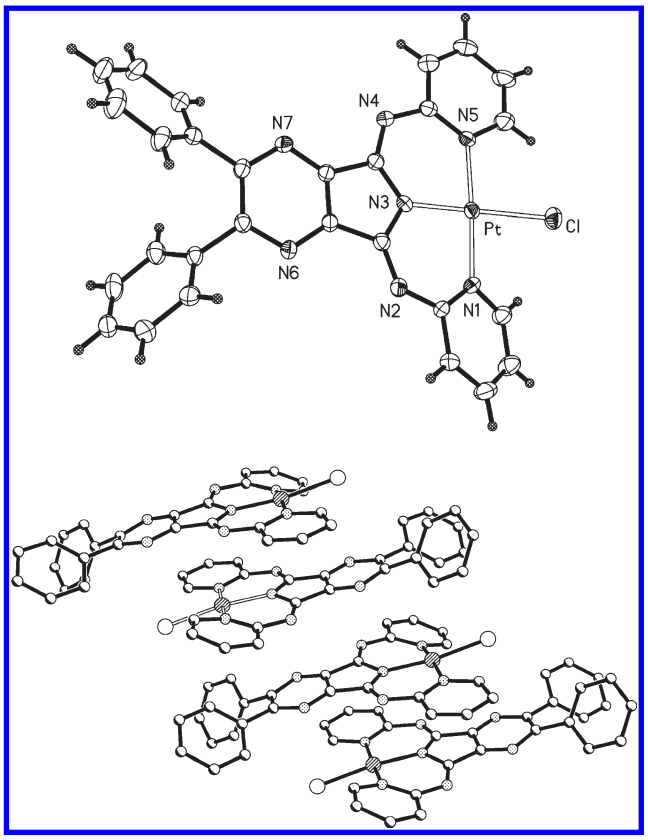

Figure 1. ORTEP drawing (top) with an atom labeling scheme showing 30% thermal ellipsoids and a packing diagram (bottom) of complex **3**.

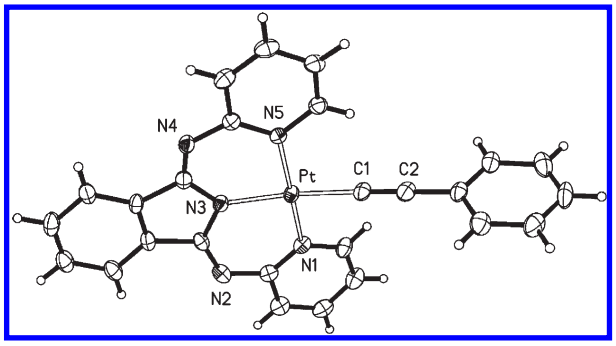

Figure 2. ORTEP drawing of complex **4** with an atom-labeling scheme showing 30% thermal ellipsoids.

Electrochemical Properties. The CVs of **1**−**11** in a 0.1 M (Bu^n_4N)(PF_6)/dichloromethane solution displayed an irreversible anodic wave at +0.63 to +1.04 V and two quasi-reversible reduction waves at −1.34 to −2.06 V vs Fc^+/Fc. The electrochemical data for complexes **1**−**11**, together with the free ligands HL1−HL3, are summarized in Table 3. The CV of **4** in a 0.1 M (Bu^n_4N)(PF_6)/dichloromethane solution is depicted in Figure 4. The free ligands HL1−HL3 display one or two irreversible reduction waves and follow the order HL2 (−2.00 V) → HL1 (−1.88 V) → HL3 (−1.65 and −2.06 V). This is in accordance with the trend of the absorption spectra and the highest occupied molecular orbital (HOMO)−lowest unoccupied molecular orbital (LUMO) energy gap (vide infra). A detailed explanation is given in the UV−Vis Absorption Spectra section.

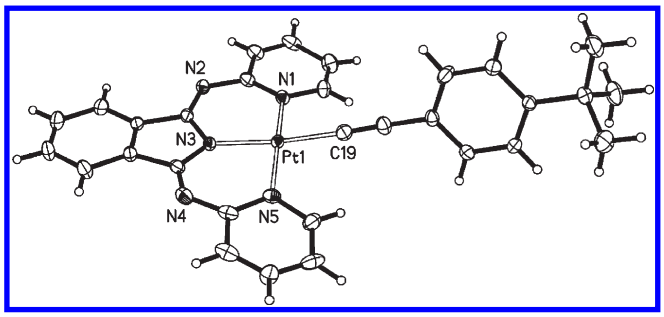

Figure 3. ORTEP drawing of complex **6** with an atom-labeling scheme showing 30% thermal ellipsoids.

Table 3. Electrochemical Data for **1**−**11**[a] in a 0.1 M (Bu^n_4N)(PF_6)/Dichloromethane Solution[a]

complex	E_{ox} (V)[b]	E_{red1} (V)	E_{red2} (V)
HL1[c]			−1.88
HL2[c]			−2.00
HL3[c]		−1.65	−2.06
1	0.91	−1.55	−1.86
2	0.90	−1.64	−1.92
3	1.04	−1.34	−1.60
4	0.67	−1.64	−1.96
5	0.68	−1.63	−1.97
6	0.67	−1.62	−1.97
7	0.70	−1.64	−1.97
8	0.65	−1.64	−1.97
9	0.68	−1.62	−1.96
10	0.63	−1.70	−2.00
11	0.74	−1.38	−1.68

[a] Potential data in volts vs Fc^+/Fc are from single-scan CVs recorded at 25 °C in a 0.1 M dichloromethane/(Bu_4N)(PF_6) solution. [b] This redox wave is irreversible, and E_{ox} is the potential of the anodic peak. [c] This redox wave is irreversible, and E_{red} is the potential of the cathodic peak.

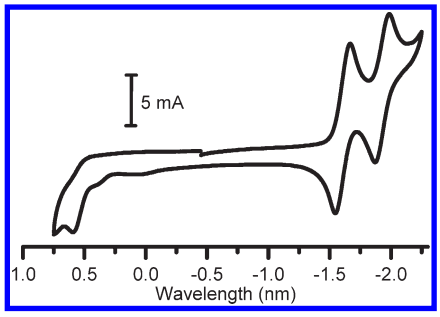

Figure 4. CV of **4** in a 0.1 M dichloromethane/(Bu^n_4N)(PF_6) solution. The scan rate is 100 mV s^{-1}.

As indicated in Table 3, the irreversible anodic wave of complexes **1**−**11** at +0.63 to +1.04 V is insensitive to variations in both L and alkynyl ligands. This suggests that this process arises mainly from metal-centered oxidation, mixed probably with some ligand-centered character.[11b] This is in accordance with the observation that the corresponding oxidation potential is obviously lowered in alkynylplatinum(II) complexes **4**−**10** (0.63−0.74 V) compared with those in the corresponding chloride-coordinated complexes **1** (0.91 V), **2** (0.90 V), and **3** (1.04 V) because the strong-field alkynyl ligand in alkynylplatinum(II) complexes would destabilize the dπ(Pt) orbital, leading to lower oxidation potentials for **4**−**10**. The higher platinum-based oxidation potential for **3** (1.04 V) than for **1** (0.91 V) and **2** (0.90 V) is due to the

Table 4. UV−Vis Absorption and Luminescence Data for **1**−**11** at Ambient Temperature

	medium	λ_{abs}/nm (ε/dm^3 mol^{-1} cm^{-1})	λ_{max}/nm (τ_{em}/μs)	ϕ_{em}/%
1	CH_2Cl_2	249 (48 270), 277 (30 470), 347 (19 990), 385 (11 000), 468 (11 300), 495 (11 260)	631 (0.96)	0.54
	solid		636 (0.63)	
2	CH_2Cl_2	251 (33 100), 301 (54 700), 385 (18 950), 409 (20 270), 458 (14 100), 480 (13 900)	601 (2.98)	3.79
	solid		602 (0.27), 648sh	
3	CH_2Cl_2	268 (35 470), 340 (34 640), 493 (9250), 514 (8760)	668 (0.28)	0.06
	solid		602sh, 660 (0.55), 720sh	
4	CH_2Cl_2	251 (46870), 280 (45650), 350 (19060), 472 (8910), 493 (8910)	625 (0.57)	0.67
	solid (black)		598, 760 (< 0.01)	
5	CH_2Cl_2	251 (46 870), 277 (40 300), 350 (17 480), 472 (8910), 493 (8900)	625 (0.51)	0.70
	solid (black)		594, 747 (< 0.01)	
	solid (red)		637 (0.48), 690sh	
6	CH_2Cl_2	249 (47 400), 278 (48 300), 348 (17 470), 378 (11 600), 472 (8520), 494 (7970)	630 (0.21)	0.36
	solid		617 (0.24), 666sh	
7	CH_2Cl_2	251 (37 400), 278 (23 300), 367 (30 720), 463 (9320), 489 (9490)	612 (2.37)	3.05
	solid		616 (0.05), 671sh	
8	CH_2Cl_2	250 (44 200), 279 (46 870), 349 (17 600), 471 (7710), 496 (7700)	635 (0.05)	0.10
	solid		650 (0.14)	
9	CH_2Cl_2	251 (46 370), 287 (43 950), 349 (19 560), 468 (10 130), 490 (10 130)	614 (1.66)	2.86
	solid		602 (0.05), 656sh	
10	CH_2Cl_2	302 (61 970), 312 (59 520), 384 (21 470), 408 (21 700), 462 (10 640), 481 (10 610)	605 (1.18)	3.79
	solid		594 (0.22)	
11	CH_2Cl_2	269 (43 410), 344 (35 250), 491 (6200), 515 (5780)	681 (0.05)	0.03
	solid		weak	

electron-deficient nature of L3, making oxidation of **3** more difficult than that of **1** and **2**.

Because the reduction potentials (Table 3) are dependent on the L ligand but insensitive to the R substituents on the phenyl ring in the alkynyl ligands HC≡CC_6H_4R-4, it is suggested that the two quasi-reversible couples originate most likely from L ligand-based reductions. This is supported by DFT calculations, in which the LUMO is found to be mainly derived from the π^* orbital localized on the L ligand (vide infra). This assignment is also in line with the observation that **1**, **2**, and **4**−**10** show more negative reduction potentials than **3** and **11** because the electron-deficient substituents on the L3 ligand would decrease the π^*(L3)-orbital energy, making reduction easier for **3** and **11**. The reduction potentials of **1**−**3** are in the order of **2** (−1.64 and −1.92 V) → **1** (−1.55 and −1.86 V) → **3** (−1.34 and −1.60 V), and those of **6**, **10**, and **11** with the same acetylide ligand but different tridentate L ligands follow **10** (−1.70 and −2.00 V) → **6** (−1.62 and −1.97 V) → **11** (−1.38 and −1.68 V). The smaller reduction potentials for **3** (or **11**) than for **1** (or **6**) and **2** (or **10**) result most likely from the better π-accepting capability because of the electron-deficient character of the L3 ligand, making **3** (or **11**) receive an electron more readily. The more negative reduction potentials for **2** (or **10**) than for **1** (or **6**) can be assigned to the fact that the HOMO−LUMO gap is **2** (or **10**) > **1** (or **6**) (vide infra), making it more difficult for **2** (or **10**) to receive an electron.

UV−Vis Absorption Spectra. The UV−vis absorption spectral data of **1**−**11** are presented in Table 4. The electronic absorption spectra of **1**−**11** are featured with high-energy bands below 300 nm, middle-energy bands at 300−380 nm, and low-energy absorption bands beyond 420 nm. As suggested from DFT calculations (vide infra), the high-energy bands result primarily from singlet intraligand (^{1}IL) transitions of the L and acetylide ligands. The middle-energy absorption bands can be ascribed to predominant a $\pi \rightarrow \pi^*$ (L) ^{1}IL transition, mixed with some character from 5d(Pt) → π^*(L) singlet metal-to-ligand charge-transfer (^{1}MLCT) and p(Cl)/π(C≡CC_6H_4R-4) → π^* (L) ligand-to-ligand charge-transfer (LLCT) states. The low-energy bands at 420−560 nm result from $\pi \rightarrow \pi^*$(L) ^{1}IL and 5d(Pt) → π^*(L) ^{1}MLCT transitions mixed with a minor contribution from the p(Cl) → π^*(L) ^{1}LLCT state for chloride-coordinated complexes **1**−**3**. Upon substitution of chloride with acetylide ligands in **4**−**11**, the low-energy absorption bands are mainly contributed by the ^{1}IL and ^{1}MLCT states, together with an increased character from the π(C≡CC_6H_4R-4) → π^*(L) ^{1}LLCT state.

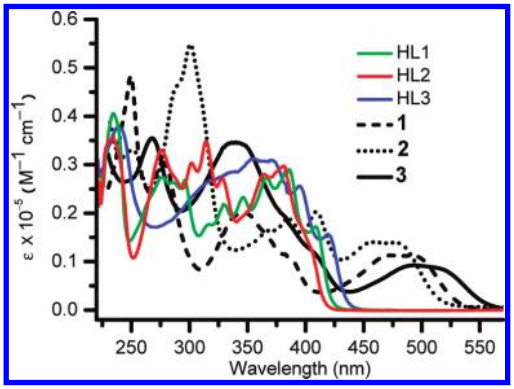

Figure 5. UV−vis absorption spectra of HL1−HL3 and **1**−**3** in dichloromethane solutions ($c = 2 \times 10^{-5}$ M) at room temperature.

Figure 5 depicts the UV−vis absorption spectra of HL1−HL3 and **1**−**3** in dichloromethane solutions at ambient temperature. Compared with those in ligands HL1−HL3 (380−410 nm), the absorption maxima of low-energy bands in complexes **1**−**3** (480−520 nm) are significantly red-shifted to a shorter-wavelength region. This is assignable to spin−orbit coupling from the heavy-atom effect of the platinum(II) ion as well as a 5d(Pt) → π^*(L) MLCT transition upon deprotonated L1−L3 binding to the platinum(II) ion. It is intriguing that the low-energy absorption wavelength of the free HL ligand in the near-UV region exhibits the order HL2 (380 and 396 nm) < HL1 (386 and 408 nm) < HL3 (395 and 420 nm), although HL2 is more extensively conjugated than HL1. The higher wavelength and lower energy of absorption features for HL3

than for HL1 and HL2 result most likely from the better π-accepting capability because of the electron-deficient character of HL3.

The absorption wavelength trend of HL2 (380 and 396 nm) < HL1 (386 and 408 nm) is unexpected and in drastic contrast with the general principle that the absorption energy is always decreased as a result of increased conjugation.[31] Although the conjugated system of HL2 is larger than that of HL1, the absorption energy of HL2 is higher than that of HL1. To understand the unexpectedly abnormal absorption trend, a DFT calculation was performed for HL1 and HL2.

The conjugate system for the ligand HL can be regarded as consisting of two electronically very different structural moieties, one being a pure carbon moiety (phenylene for HL1 or naphthylene for HL2) and the other containing N-heteroatoms (the same for HL1 and HL2). As depicted in Figure S4 (Supporting Information), the HOMO for HL1 or HL2 is predominantly contributed by an N-heteroatomic moiety so that the HOMO level of HL1 (−5.9651 eV) is close to that of HL2 (−5.9553 eV). The LUMO, however, is resident on both N-heteroatomic and pure carbon moieties. As indicated in the diagrams of the LUMO (Figure S4, Supporting Information) for HL1 and HL2, although the naphthylene in HL2 has a more extended system than the phenylene in HL1, the naphthylene in HL2 contributes more antibonding π^* composition so as to afford a higher level of LUMO for HL2 (−1.9957 eV) compared with that for HL1 (−2.0896 eV). This leads to a larger HOMO−LUMO gap for HL2 (3.9596 eV) than that for HL1 (3.8755 eV), thus explaining the absorption trend of HL1 and HL2.

To understand this more clearly, Figure S5 (Supporting Information) shows a proposed schematic illustration of the relevant orbital interaction. In this schematic illustration, we made an unconventional assumption that the π and π^* orbitals of the N-containing moiety are higher in energy than the π and π^* orbitals of the pure carbon moiety (phenylene or naphthylene). This unconventional assumption is based on the fact that the HOMOs of HL1 and HL2 are mainly contributed by the highest π orbital from the N-containing moiety while the LUMOs of HL1 and HL2 are significantly contributed by the lowest π^* orbital of the pure carbon moiety (phenylene or naphthylene). Our molecular orbital calculations on HL1 and HL2 show that the HOMO for HL1 or HL2 corresponds to the out-of-phase combination between the π orbitals of the pure carbon moiety and the N-containing moiety while the LUMO is the in-phase combination of the π^* orbitals of the two moieties. The π orbitals of the N-containing moiety and the pure carbon moiety (phenylene or naphthylene) differ significantly in their orbital energies so that the orbital interaction between them is less significant and the HOMOs for HL1 and HL2 are mainly contributed by π orbitals from the N-containing moiety. As a consequence, the HOMOs for both HL1 and HL2 have similar orbital energies (Figure S5, Supporting Information). In contrast, the LUMOs for HL1 and HL2 arise from π^*-orbital interaction between the pure carbon moiety and the N-containing one, in which the π^* orbitals of the two moieties have similar orbital energies. Compared with that of the naphthylene in HL2, the π^* orbital of the phenylene in HL1 is closer in energy to the π^* orbital of the N-containing moiety. As a result, the orbital interaction is more significant for HL1 so as to give a lower energy of the LUMO, thus leading to a smaller HOMO−LUMO gap in HL1, as depicted in Figure S5 (Supporting Information). Although the naphthylene in HL2 has a larger conjugated system, the energy match between the π^* orbitals of the naphthylene and the π^* orbitals of the N-containing moiety is worse than that in HL1 so as to give a less significant orbital interaction, thus resulting in a higher level of the LUMO and a larger HOMO−LUMO gap in HL2. We have to point out that in the schematic illustration shown in Figure S5 (Supporting Information) we purposely aligned the π- and π^*-orbital energy levels of the N-containing moiety to fit the resulting orbital levels of HL1 and HL2.

In the same trend as ligands L1−L3, the absorption maxima of the low-energy bands in platinum(II) complexes **1**−**3** (Figure 5) follow **2** (458 and 480 nm) < **1** (468 and 495 nm) < **3** (493 and 514 nm), which is in accordance with the HOMO−LUMO gap with **2** (3.54 eV) > **1** (3.46 eV) > **3** (3.31 eV) from DFT calculations (vide infra). Similarly, the low-energy absorption bands of **6**, **10**, and **11** (Figure S4, Supporting Information) with the same acetylide ligand [(4-*tert*-butylphenyl)acetylide] but different L ligands follow **10** (462 and 481 nm) < **6** (472 and 494 nm) < **11** (491 and 515 nm). Thus, the low-energy absorption bands can be modulated to some extent by modification of the L ligands. By a comparison of the low-energy absorption bands in L1 complexes **4**−**9** containing C≡C(C_6H_4)R-4 with different electron-donating or -withdrawing substituent R, it is found that the lowest-lying absorption bands are insensitive to the R substituent on the phenyl ring in the alkynyl ligands HC≡CC_6H_4R-4 probably because of the predominant contribution of the $\pi \rightarrow \pi^*$(L) ^{1}IL state to the absorption character, as revealed by DFT calculations (vide infra). This is in contrast with that of alkynylplatinum(II) complexes of tpy or bzimpy,[2,10] in which low-energy absorption bands are usually tunable to some extent by the introduction of an electron-donating or -withdrawing substituent in the phenylacetylide ligand.

The UV−vis electronic spectra of **1** (Figure S6, Supporting Information) and **4** (Figure S7, Supporting Information) in different solutions at ambient temperature indicate that the low-energy absorption bands exhibit a small shift (10−20 nm) depending on the solvents. The absorbance of the low-energy bands displays a linear relationship with the concentration from 1×10^{-6} to 5×10^{-4} M in dichloromethane solutions. Once the solution concentration is higher than 5×10^{-4} M, the UV−vis absorption spectra of **1** and **4** do not obey Lambert−Beer's law (Figure S8, Supporting Information).

Luminescence Properties. The luminescence data including emission wavelengths, lifetimes, and quantum yields of **1**−**11** are summarized in Table 4. Upon irradiation of these complexes with near-UV light, complexes **1**−**11**

(31) (a) Vala, M.; Vynuchal, J.; Toman, P.; Weiter, M.; Lunak, S., Jr. *Dyes Pigments* **2010**, *84*, 176–182. (b) Wasserberg, D.; Meskers, S. C. J.; Janssen, R. A. J.; Mena-Osteritz, E.; Bauerle, P. *J. Am. Chem. Soc.* **2006**, *128*, 17007–17017. (c) Adachi, M.; Nagao, Y. *Chem. Mater.* **1999**, *11*, 2107–2114. (d) Lee, Y. H.; Kim, Y. S. *Thin Solid Films* **2007**, *515*, 5079–5083.

show bright room-temperature luminescence in both solid states and fluid dichloromethane solutions with microsecond or submicrosecond lifetime ranges. Large Stokes shifts together with long emissive lifetimes reveal that they are phosphorescent in nature with triplet excited states. In most cases, the emission spectra in solid states at 298 K exhibit well-resolved vibronic-structured bands (Figure S9, Supporting Information) with vibrational progressional spacings in the range of 1160−1460 cm^{-1} (Table 4), characteristic of the vibrational stretching frequencies of the aromatic C=C and C=N modes of the tridentate N-heterocyclic L ligands. The emission quantum yields in degassed dichloromethane solutions are in the range of 0.03−3.79% at ambient temperature (Table 4). The room-temperature emission spectra of **1** (Figure S15, Supporting Information) in various solvents including THF, *N*,*N*-dimethylformamide, toluene, CH_2Cl_2, and CH_3CN suggest that they are insensitive to the solution character. Upon excitation of the dichloromethane solution of **4** at λ_{ex} = 460 nm, the room-temperature emission at 625 nm becomes stronger and stronger with increasing concentration from 1×10^{-6} to 1×10^{-4} M. At concentrations $>10^{-4}$ M, the dichloromethane solution of **4** (Figure S16, Supporting Information) displays a self-quenching phenomenon, but excimeric emission is undetectable in the range of 300−900 nm. Nevertheless, the excitation maxima of **4** (Figure 17, Supporting Information) in dichloromethane solutions at high concentrations ($>10^{-4}$ M) are gradually red-shifted from 485 nm (1×10^{-4} M) to 550 nm (1×10^{-3} M) probably because of an increasing contribution from the π(C≡CC_6H_4R-4) → π^*(L) ^{3}LLCT state.

It has been demonstrated that most of the [Pt(N^N^N)Cl]$^+$ complexes with N^N^N = tpy,[32,33] bpp,[2f] or bzimpy[2d] are nonemissive or weakly luminescent in fluid solutions at ambient temperature, although they are always emissive in solid states. In striking contrast, complexes **1**−**3** show bright luminescence with structureless emission bands at 631, 601, and 668 nm (Figure 6), respectively, in fluid dichloromethane solutions at 298 K, arising primarily from $^3[\pi \rightarrow \pi^*(L)]$ ^{3}IL and ^{3}[5d(Pt) → π^*(L)] ^{3}MLCT triplet excited states as revealed from DFT calculations (vide infra). It is obvious that, compared with that of **1**, the emission of **2** is blue-shifted, whereas that of **3** exhibits a red shift. The emission wavelength **2** (601 nm) < **1** (631 nm) < **3** (668 nm) is well consistent with that of the lowest-energy absorption bands and the energy trend of the HOMO−LUMO gap with **2** > **1** > **3** (vide infra). It is worth noting that the measured emission energy **2** (2.06 eV) > **1** (1.96 eV) > **3** (1.86 eV) coincides reasonably with the calculated triplet excitations **2** (2.16 eV) > **1** (2.06 eV) > **3** (1.93 eV) from DFT calculations (vide infra).

Upon substitution of the coordinated chloride in **1**−**3** with an acetylide ligand in **4**−**11**, the emission origins become [$\pi \rightarrow \pi^*$(L)] ^{3}IL and [5d(Pt) → π^*(L)] ^{3}MLCT states mixed with an enhanced contribution from the π(C≡CC_6H_4R-4) → π^*(L) ^{3}LLCT transition, as suggested from DFT calculations (vide infra). For (4-*tert*-butylphenyl)acetylide complexes **6**, **10**, and **11** with different L ligands, the emission wavelength (Figure S10, Supporting Information) follows **10** (615 nm) < **6** (630 nm) < **11** (681 nm) like that for the lowest-energy absorption bands. Similarly, this can be reasonably interpreted by the fact that the π^* energy of L2 is enhanced whereas that of L3 is reduced compared with that of L1. For complexes **4**−**9** with the same L1 ligand but different acetylide ligands, the emission shows some dependence on the substituent R in the acetylide ligand C≡CC_6H_4R-4. As depicted in Figure S14 (Supporting Information), the emission of **7** (612 nm) with R = NO_2 is blue-shifted whereas that of **8** (635 nm) with R = OCH_3 displays a red shift compared with that of **4** (625 nm). Obviously, the introduction of an electron-withdrawing substituent to the phenylacetylide would lower the energy of the 5d(Pt) and π(C≡CC_6H_4R-4) orbitals, thus increasing the HOMO−LUMO gap of the 5d(Pt) → π^*(L) ^{3}MLCT and π(C≡CC_6H_4R-4) → π^*(L) ^{3}LLCT states. In contrast, the introduction of an electron-donating substituent would reduce the HOMO−LUMO gap of the ^{3}MLCT and ^{3}LLCT transitions, thus inducing a red shift of the emission.

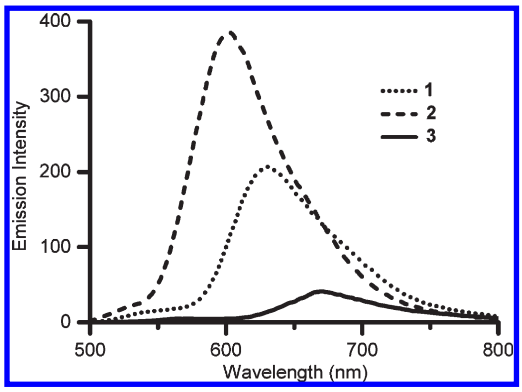

Figure 6. Emission spectra of **1** (dotted line), **2** (dashed line), and **3** (solid line) in degassed dichloromethane solutions ($c = 2 \times 10^{-5}$ M) at room temperature (λ_{ex} = 460 nm).

Complex **5** with (4-fluorophenyl)acetylide affords two differently colored crystalline forms. The red form exhibits bright-red luminescence at 637 nm (Figure S12, Supporting Information) analogous to that measured in a fluid dichloromethane solution, arising most likely from the $\pi \rightarrow \pi^*$(L) ^{3}IL and 5d(Pt) → π^*(L) ^{3}MLCT triplet excited states mixed with some π(C≡CC_6H_4R-4) → π^*(L) ^{3}LLCT character. The black form, however, is weakly luminescent at 747 nm, with a significant red shift relative to that of the red form. The differently colored crystalline forms for a given platinum(II) complex are likely associated with the difference in the crystal packing in the stacking of planar platinum(II) moieties,[7,8] although the crystal structures of both forms have not been characterized by X-ray crystallography. It is likely that a significant red shift for the black form results from a change in the emissive character from ^{3}MLCT to ^{3}MMLCT (metal−metal-to-ligand charge-transfer) state probably because of the presence of significant Pt−Pt and/or π−π interactions in the black form.[7,34−36]

(32) Lai, S.-W.; Chan, M. C. W.; Cheung, K.-K.; Che, C.-M. *Inorg. Chem.* **1999**, *38*, 4262–4267.
(33) Büchner, R.; Field, J. S.; Haines, R. J. *Inorg. Chem.* **1997**, *36*, 3952–3956.
(34) Field, J. S.; Gertenbach, J. A.; Haines, R. J.; Ledwaba, L. P.; Mashapa, N. T.; McMillin, D. R.; Munro, O. Q.; Summerton, G. C. *Dalton Trans.* **2003**, 1176–1180.
(35) Miskowski, V. M.; Houlding, V. H. *Inorg. Chem.* **1991**, *30*, 4446–4452.
(36) Yam, V. W. W.; Chan, K. H. Y.; Wong, K. M. C.; Zhu, N. Y. *Chem.—Eur. J.* **2005**, *11*, 4535–4543.

Table 5. Partial Molecular Orbital Compositions (%) in the Ground State for **1** in Dichloromethane Media under TD-DFT Calculations and the Absorptions and Emission Transitions for **1** in Dichloromethane Media Calculated by the TD-DFT Method

		MO contribution (%)		
orbital	energy (eV)	Pt	L1	Cl
LUMO+1	−1.3576	3.1	96.8	0.1
LUMO	−2.5421	3.7	96.3	0.0
HOMO	−5.9993	34.0	55.6	10.4
HOMO−1	−6.7215	26.4	55.4	18.3
HOMO−3	−7.0138	89.5	9.5	0.9
HOMO−4	−7.1292	30.6	44.5	24.9
HOMO−5	−7.2826	53.1	46.4	0.5

	transition	contribution (%)	*E* [nm (eV)]	OS	assignment	measured value (nm)
T1	HOMO → LUMO	93	601 (2.06)	0.0000	^{3}IL/^{3}MLCT/^{3}LLCT	631
S1	HOMO → LUMO	91	466 (2.66)	0.1312	^{1}IL/^{1}MLCT/^{1}LLCT	468, 495
S4	HOMO−1 → LUMO	59	358 (3.47)	0.2283	^{1}IL/^{1}MLCT/^{1}LLCT	380 (sh)
	HOMO−3 → LUMO	37			^{1}MLCT	
S8	HOMO−5 → LUMO	63	311 (3.99)	0.1978	^{1}IL/^{1}MLCT	34
	HOMO−4 → LUMO	15			^{1}IL/^{1}MLCT/^{1}LLCT	
S22	HOMO−4 → LUMO+1	72	252 (4.92)	0.2092	^{1}IL/^{1}MLCT/^{1}LLCT	277

Table 6. Partial Molecular Orbital Compositions (%) in the Ground State and the Absorptions and Emission Transitions for **4** in Dichloromethane Media Calculated by the TD-DFT Method

		MO contribution (%)		
orbital	energy (eV)	Pt	L1	C≡CC_6H_5
LUMO+3	−0.7388	3.5	95.9	0.6
LUMO+1	−1.2466	1.8	98.2	0.0
LUMO	−2.4548	3.8	96.2	0.0
HOMO	−5.8064	12.7	11.9	75.4
HOMO−1	−5.8475	33.9	46.0	20.1
HOMO−2	−6.4655	12.5	62.1	25.4
HOMO−6	−7.1958	54.5	45.5	0.0

	transition	contribution (%)	*E* [nm (eV)]	OS	assignment	measured value (nm)
T1	HOMO−1 → LUMO	84	600 (2.07)	0.0000	^{3}IL/^{3}MLCT/^{3}LLCT	627
	HOMO−2 → LUMO	16			^{3}IL/^{3}MLCT/^{3}LLCT	
S1	HOMO−1 → LUMO	94	474 (2.62)	0.1047	^{1}IL/^{1}MLCT/^{1}LLCT	472, 493
	HOMO−2 → LUMO	6			^{1}IL/^{1}MLCT/^{1}LLCT	
S3	HOMO−2 → LUMO	95	370 (3.35)	0.3305	^{1}IL/^{1}MLCT/^{1}LLCT	shoulder
S10	HOMO−6 → LUMO	88	310 (3.99)	0.1657	^{1}MLCT/^{1}ILCT	350
S20	HOMO−2 → LUMO+1	68	275 (4.52)	0.4205	^{1}IL/^{1}MLCT/^{1}LLCT	280
	HOMO−1 → LUMO+3	23			^{1}IL/^{1}MLCT/^{1}LLCT	

Theoretical Studies. DFT calculations were carried out for **1**−**4** and **6** to gain better insight into the electronic and spectroscopic properties as well as the nature of absorption and emission origins of these platinum(II) complexes. On the basis of the ground-state optimized geometry, 80 singlet and 6 triplet excited states for the related complexes were calculated at the PBE1PBE/LANL2DZ[6-31G(d,p)] level with the TD-DFT, in which the solvent effect (CH_2Cl_2 as the solvent) with the CPCM approach is taken into account. The relative compositions of the different energy levels in terms of the composing fragments and the absorption transition characters are summarized in Table 5 for **1**, in Table 6 for **4**, and in Tables S2−S7 (Supporting Information) for **2**, **3**, and **6**. Electron-density diagrams of the frontier molecular orbitals involved in the absorption spectra of **1**−**4** and **6** in dichloromethane are depicted in Figures S19−S23 (Supporting Information). The energy diagrams of important frontier orbitals and the single electron-density diagrams of HOMOs and LUMOs involved in the absorptions for **1**−**4** and **6** are shown in Figure 7.

Complexes **1**−**4** and **6** display similar LUMO features, with the π^* orbitals mainly centered on the tridentate chelating ligand L. For **1**−**3**, the HOMO is primarily contributed from the platinum atom (ca. 34%) and the chelating L ligand (55−57%), with minor contribution from the coordinated chloride (ca. 10%). The HOMO−1 is mainly composed of the chelating ligand L with 55.4% (Table 5), 95.3% (Table S2, Supporting Information), and 97.3% (Table S4, Supporting Information) contributions for **1**−**3**, respectively. In contrast to the compositions of the HOMOs in **1**−**3**, those in **4** and **6** with acetylide ligands are quite different. The HOMO is mainly localized on the phenylacetylide for **4** (75.4%; Table 6) and (4-*tert*-butylphenyl)acetylide for **6** (69.0%) (Table S6, Supporting Information). The HOMO−1 is resident on the platinum atom and L and acetylide ligands with 33.9%, 46.0%, and 20.1% compositions for **4** (Table 6) and 29.5%, 42.3%, and 28.2% contributions for **6** (Table S6, Supporting Information), respectively.

For chloride-containing complexes **1**−**3**, the HOMO−LUMO energy gap is 3.46 eV for **1**, 3.54 eV for **2**, and 3.31 eV for **3** (Figure 7). The calculated lowest-energy absorption wavelength follows 449 nm (**2**) < 466 nm (**1**) < 490 nm (**3**), well in accordance with the corresponding

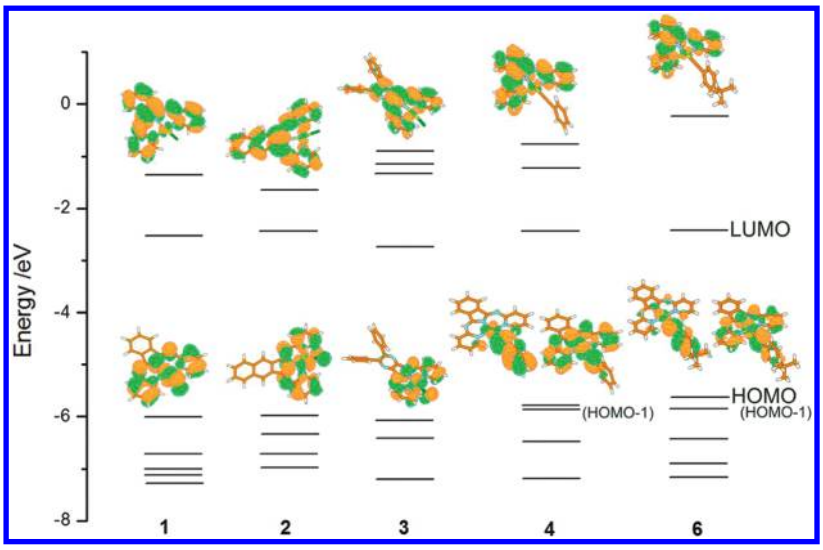

Figure 7. Diagrams of the energy levels of HOMOs and LUMOs involved in the absorptions for **1**−**4** and **6** under TD-DFT calculations.

values from the experimental measurement (Figure 4). The lowest-energy absorption (HOMO → LUMO) can be primarily assigned as $\pi \rightarrow \pi^*$(L) ^{1}IL and 5d(Pt) → π^*(L) ^{1}MLCT transitions, mixed with minor π(Cl) → π^*(L) ^{1}LLCT character. The lowest-lying triplet transitions at 601 nm for **1** (Table 5), 574 nm for **2** (Table S3, Supporting Information), and 643 nm for **3** (Table S5, Supporting Information) corresponding to excitation of HOMO → LUMO are in reasonable agreement with the experimentally measured emissions (631 nm for **1**, 601 nm for **2**, and 668 nm for **3**) in fluid dichloromethane solutions, typical of $^3[\pi \rightarrow \pi^*(L)]$ ^{3}IL and ^{3}[5d(Pt) → π^*(L)] ^{3}MLCT character, mixed with a minor contribution from the $^3[\pi(Cl) \rightarrow \pi^*(L)]$ ^{3}LLCT state. As a result, the emission origins of **1**−**3** coincide well with the low-energy absorption character mentioned previously. The main singlet and triplet vertical excitation energies for each complex from TD-DFT calculations agree well with the experimental values (Figures S24−28, Supporting Information).

As indicated in Tables 6 and S7 (Supporting Information), the calculated lowest singlet absorptions at 474 nm for **4** (HOMO−1 → LUMO) and 492 and 463 nm for **6** (HOMO−1 → LUMO and HOMO → LUMO) result from an admixture of the $[\pi \rightarrow \pi^*(L)]$ ^{1}IL, [5d(Pt) → π^*(L)] ^{1}MLCT, and $[\pi(C{\equiv}CC_6H_4R\text{-}4) \rightarrow \pi^*(L)]$ ^{1}LLCT states. Figure 8 depicts the measured (solid line) and calculated (dashed line) absorption spectra of **6** simulated with Gaussian curve. The triplet excitations at 600 nm for **4** (Table 6) and 603 nm for **6** (Table S7, Supporting Information) from the HOMO−1 → LUMO (84% for **4** and 65% for **6**) transition coincide reasonably with the measured emissions at 625 nm for **4** and 630 nm for **6** in fluid chloromethane solutions. The emission transitions are most likely composed of an admixture of the $^3[\pi \rightarrow \pi^*(L1)]$ ^{3}IL, ^{3}[5d(Pt) → π^*(L1)] ^{3}MLCT, and $^3[\pi(C{\equiv}CC_6H_4R\text{-}4) \rightarrow \pi^*(L1)]$ ^{3}LLCT states. By comparison with the low-energy transition character in **1**, it is found that substitution of chloride with an acetylide ligand in **4** and **6** increases obviously the contribution from the $\pi(C{\equiv}CC_6H_4R\text{-}4) \rightarrow \pi^*$(L1) LLCT state.

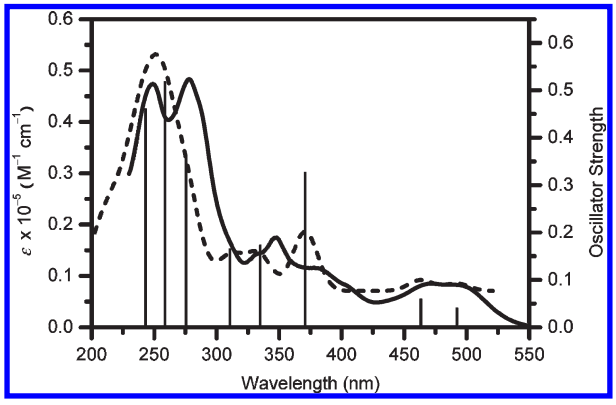

Figure 8. Measured (solid line) and calculated (dashed line) absorption spectra of **6** simulated with Gaussian curve. The singlet excited states calculated are shown as vertical bars with heights equal to the oscillator strength.

Conclusions

A series of neutral platinum(II) complexes with monoanionic tridentate BPI derivatives were synthesized and characterized. As revealed from X-ray crystallography, the platinum(II) center adopts a more perfect square-planar geometry than that in platinum(II) terpyridine complexes. The square-planar platinum(II) complexes with a terminally coordinated chloride or phenylacetylide display bright solution luminescence at ambient temperature, originating mainly from $^3[\pi \rightarrow \pi^*(L)]$ ^{3}IL and ^{3}[5d(Pt) → π^*(L)] ^{3}MLCT triplet excited states, as verified by DFT calculations. It is demonstrated that substitution of a coordinated chloride in Pt(L)Cl complexes with a phenylacetylide induces a significantly enhanced contribution from the $^3[\pi(C{\equiv}CC_6H_4R\text{-}4) \rightarrow \pi^*(L)]$ ^{3}LLCT state. The solution luminescence can be fine-tuned by modification of the substituents in both L and phenylacetylide ligands. The low-energy absorption and emission energy follow **2** > **1** > **3** and **10** > **6** > **11**, respectively, which coincide well with the HOMO−LUMO gap with **2** > **1** > **3** from DFT calculations and can be reasonably interpreted by the π^* energy level of the tridentate L ligands with L2 > L1 > L3.

Acknowledgment. We are thankful for financial support from the NSFC (Grants 20625101, 20633020, 20821061, and 20931006), the 973 project (2007CB815304) from MSTC, and the NSF of Fujian Province (Grants 2008I0027 and 2008F3117). We are grateful to Professor Zhenyang Lin at the Hong Kong University of Science and Technology for his helpful discussion and suggestions in the revision of this manuscript.

Supporting Information Available: Figures giving additional UV−vis and emission spectra, tables and figures giving DFT calculation data, and X-ray crystallographic file in CIF format for the structure determination of **1**, **4**, and **6**. This material is available free of charge via the Internet at http://pubs.acs.org.